https://doi.org/10.1016/j.ijrefrig.2016.07.011

Thermodynamic assessment of an integrated molten carbonate fuel cell and absorption refrigerator hybrid system for combined power and cooling applications

Houcheng Zhang [a, b, *], Bin Chen [a], Haoran Xu [a], Meng Ni [a]

[a] *Department of Building and Real Estate, The Hong Kong Polytechnic University, Hong Kong, China*

[b] *Department of Microelectronic Science and Engineering, Ningbo University, Ningbo 315211, China*

Abstract: A hybrid system is proposed to harvest the waste heat released in MCFC through integrating an absorption refrigerator as a bottoming cycle. A thermo-electrochemical model is used to describe the main irreversible losses in the system. The operating current density interval of the MCFC that enables the bottoming absorption refrigerator to effectively cool is determined. Numerical expressions for the equivalent power output and efficiency are derived to evaluate the performance of the hybrid system under different operating conditions. Compared to the stand-alone MCFC, the maximum power density and the corresponding efficiency of the hybrid system are found to be increased by 3.2% and 3.8%, respectively. The general performance characteristics and optimum operating regions for the hybrid system are revealed. Comprehensive parametric analyses are conducted to investigate how the hybrid system performance depends on various physical properties and working conditions such as working fluid internal irreversibility inside the absorption refrigerator, heat transfer coefficients, some thermodynamic losses related parameters, and the operating current density, temperature and pressure of the MCFC.

Keywords: Molten carbonate fuel cell; Absorption refrigerator; Hybrid system; Irreversible loss; Thermodynamic assessment

[*]Corresponding author. Tel.: +86 574 87600770; Fax: +86 574 87600744. E-mail: zhanghoucheng@nbu.edu.cn.

Nomenclature

A	Effective polar plate area of the MCFC (m^2)
A_L	Heat-transfer area between the MCFC and the environment (m^2)
A_R	Overall heat-transfer area of the absorption refrigerator (m^2)
A_0	Total heat-transfer area of the condenser and absorber (m^2)
A_c	Heat-transfer area of the evaporator (m^2)
A_h	Heat-transfer area of the generator (m^2)
A_{re}	Heat-transfer area of regenerator (m^2)
b_1	Ratio between K_h and K_0
b_2	Ratio between K_h and K_c
c_1, c_2	Integrated parameters in Eq. (14) (W m^{-2} K^{-1})
E	Equilibrium potential (V)
E_0	Ideal standard potential (V)
E_{act}	Activation energy (J mol^{-1})
F	Faraday's constant (C mol^{-1})
$(-\Delta \dot{H})$	Total energies supplied to the hybrid system per unit time (J s^{-1})
Δh	Molar enthalpy change of the electrochemical reactions (J mol^{-1})
I	Operating electric current through the cell (A)
I_r	Internal irreversibility
j	Operating current density (A m^{-2})
j_0	Exchange current density (A m^{-2})
j_C	Lower bound operating current density of the MCFC (A m^{-2})

j_M	Allowable maximum current density of the MCFC (A m^{-2})
j_S	Stagnation operating current density of the MCFC (A m^{-2})
j_P	Operating current density at $P^*_{\max}$ (A m^{-2})
K	Heat-transfer coefficient in Eqs. (8) and (9) (J m^{-2} K^{-1} s^{-1})
K_L	Heat-leakage coefficient (J m^{-2} K^{-1} s^{-1})
K_{re}	Heat-transfer coefficient of the regenerator (J m^{-2} K^{-1} s^{-1})
n_e	Number of electrons involved per electrochemical reaction
P	Power output (W)
P_{AR}	Equivalent power output of the absorption refrigerator (W)
P^*	Power density (W m^{-2})
P^*_C	Power density at j_C (W m^{-2})
P^*_M	Power density at j_M (W m^{-2})
$P^*_{\max}$	Maximum power density of the hybrid system (W m^{-2})
p_i	Partial pressures of specie i (atm)
q_L	Heat-leakage rate from the MCFC to the environment (J s^{-1})
q_0	Total heat-transfer rate from the condenser and absorber to the environment (J s^{-1})
q_c	Heat-transfer rate from the cooled space to the evaporator (J s^{-1})
q_h	Heat-transfer rate from the MCFC to the generator (J s^{-1})
q_{re}	Heat-loss rate of the regenerator (J s^{-1})
$\boldsymbol{R}$	Universal gas constant (J mol^{-1} K^{-1})
ΔS_h	Rate of entropy flows into the working fluid at temperature T_1 (J s^{-1} K^{-1})

ΔS_c	Rate of entropy flows into the working fluid at temperature T_2 (J s^{-1} K^{-1})
ΔS_0	Rate of entropy flows out of the working fluid at temperature T_3 (J s^{-1} K^{-1})
T	Operating temperature of MCFC (K)
T_0	Temperatures of the environment (K)
T_1 , T_2, T_3	Temperatures of the working fluids in the generator, evaporator, condenser and absorber (K)
T_c	Temperature of the cooled space (K)
U_m	Overpotentials (*m* = *an*, *cat* or *ohm*) (V)

Greek symbols

ε	Effectiveness of the regenerator
η	Efficiency
η_{AR}	Efficiency of the absorber refrigerator
η_C	Efficiency at j_C
η_P	Efficiency at $P^*_{\max}$

Subscripts

an	Anode
cat	Cathode
ohm	Ohmic
AR	Absorption refrigerator

1. Introduction

Unlike conventional heat engines in which electricity is produced from chemical energy with the intermediate mechanical energy conversion, fuel cells are static energy conversion devices that directly convert the chemical energy in fuels into electricity [1, 2]. Fuel cells have the great potential to reduce greenhouse gas emissions and fossil fuel consumptions and have been considered to be one of the most promising power generation technologies [3]. MCFCs (molten carbonate fuel cells) use a molten carbonate electrolyte, which is usually a mixture of Li_2CO_3 and K_2CO_3. At anode, the input hydrogen reduces CO_3^{2-} ions in the electrolyte to form CO_2 and release two electrons. The produced CO_2 are subsequently transported to the cathode. At cathode, new CO_3^{2-} ions are formed by combing the CO_2 from the anode and the O_2 from the air with the two electrons from the external circuit thus closing the chemical and electrical loops [4]. In the existing literature, most investigations on MCFCs have focused on aspects including materials fabrication [5, 6], further understanding of electrochemical processes and transport phenomena [7, 8], stack modeling and dynamic simulation [9-11], and cell-based carbon dioxide capture [12, 13]. Up to now, MCFCs have reached a level of maturity enough for commercialization in some countries such as USA, Germany, Japan, Italy and South Korea [14].

The R&D in MCFCs has made a great progress in solving problems such as corrosion issue, short lifetime, and high cost [15-17], however, the low power density is still a drawback that restricts the wide commercialization of MCFCs [18]. To improve the power density, many efforts have made on MCFC itself by optimizing the operating conditions and system layouts or by developing more advanced materials to reduce the polarization losses [19-23]. Alternatively, the high operating temperature of MCFC provides an opportunity of cogeneration with CHP (combined heat and power)

systems to recover the waste heat for additional applications, and thus, the power density of MCFC-based cogeneration systems could be enhanced with reference to that of the stand-alone mode MCFCs [24-36]. Gas turbines are often used as the bottoming cycle for MCFCs, a number of studies are performed on MCFC-GT (MCFC-gas turbine) hybrid systems fed with different fuels using different analysis approaches at different scales [24-29]. In addition to the common gas turbine engines, some scholars discussed the feasibilities of some other bottoming thermal cycles for MCFCs [30-35]. Zhang et al. [30, 31] employed a Carnot cycle and a Braysson cycle to recover the waste heat for additional power generation and revealed the effects of some operating conditions and designing parameters on the performance of the hybrid system. Sánchez et al. [32] compared a reciprocating engine with three bottoming thermal cycles (Rankine cycle, Brayton cycle and Stirling cycle) for an MCFC and showed that the Stirling engine was an alternative competitor over conventional gas turbines. Vatani et al. [33] considered an ORC (Organic Rankine Cycle) to recover the waste heat from an IR-MCFC (internal reforming-MCFC) with two different configurations, the first configuration was that the cathode outlet provided the heat for pre-reforming process and then entered ORC, and the second configuration was that the cathode outlet was simultaneously split into two streams for ORC and pre-reforming process. The global energy and exergy efficiencies of the latter configuration were found to be 60.45% and 57.75%, respectively, which were about 3% higher than that of the first configuration. Mamaghani et al. [34] proposed an MCFC-GT-ORC (Molten Carbonate Fuel Cell-Gas Turbine-Organic Rankine Cycle) hybrid plant, 4E (energetic, exergetic, economic and environmental) analyses were performed and the multi-objective optimum solutions showed that the exergetic efficiency of the hybrid plant was about 55%, which was approximately 19.4% larger than that of the sole MCFC system. Chen et al. [35] developed a hybrid system based

on a high-temperature fuel cell and a heat engine with a unified model including Carnot, Brayton, Otto, Diesel, Atkinson, and Braysson cycles. They investigated the effects of main irreversible losses in fuel cells and heat engines on the performance of the hybrid system and determined the optimum operating region of some important performance parameters.

Refrigeration systems play a crucial role in our daily lives as they could provide human comfort and food preservation [36]. Up to now, most of the installed refrigeration systems are conventional vapor compression cooling devices, which not only use ozone-depleting working fluids but also consume electricity [37-43]. An absorption refrigerator, enables to effectively cool by using heat instead of electricity, which has been widely used for waste heat recovery and air conditioning [44-50]. Recently, Silveira et al. [51] used the waste heat contained in the exhaust gases of an MCFC to run an absorption refrigerator for electricity and cold water production synchronously. This technology was demonstrated to be feasible by energy, exergy and economic analyses. However, thereafter, seldom works done on this MCFC/absorption refrigerator hybrid system. Further development and optimization are still required in order to make this system to be economical, reliable, efficient and even market-competitive.

In this study, a hybrid system that integrates a MCFC with an absorption refrigerator to simultaneously produce electricity and cooling is established to improve the overall performance. Numerical expressions for the power output and efficiency of the hybrid system are formulated by considering multiple irreversibilities such as the electrochemical irreversible losses inside the MCFC, internal irreversibilities inside the absorption refrigerator, regeneration losses in the regenerator, and heat-transfer irreversibilites between the MCFC and the absorption refrigerator and the surroundings. The general performance characteristics and optimum operating regions of the hybrid system are

revealed, and the operating current densities of the MCFC that enable the absorption refrigerator to function will be determined. The effects of some operating conditions and design parameters on the performance of the hybrid system will be discussed through comprehensive parametric analyses.

2. System description

The hybrid system proposed in this paper consists of a MCFC, a regenerator and an absorption refrigerator, as schematically shown in Fig. 1, where the absorption refrigerator is constituted by a generator, a condenser, an evaporator and an absorber. The MCFC converts the chemical energy in the fuel into electricity and waste heat. The electricity is delivered to the external circuit and the waste heat is collected and extracted for else uses. One part of the waste heat is transferred to the generator to drive the bottoming absorption refrigerator for cooling purposes, another part is transferred to compensate the regenerative losses, and the last part is leaked into the environment. In Fig. 1, P_{MCFC} is the electric power output of the MCFC, q_h is the heat-transfer rate from the MCFC at temperature T to the working fluid in the generator at temperature T_1, q_c is the heat-transfer rate from the cooled space at temperature T_c to the working fluid in the evaporator at temperature T_2, q_0 is the total heat-transfer rate from the working fluids in the condenser and absorber at temperature T_3 to the environment at temperature T_0, q_L is the heat-leakage rate from the MCFC to the environment, and q_r is the heat loss rate in the regenerator.

To conveniently describe the main irreversible losses existing in the system, some simplifications and assumptions are made [52-55]: (1) Both MCFC and absorption refrigerator are operated under steady state conditions; (2) Operating temperature and pressure are uniform and constants in the MCFC; (3) Electrochemical reactions are completely proceed; (4) Internal electric current and fuel crossover are negligible; (5) Working fluids in the absorber and condenser shares the same

temperature; (6) Working fluids in the absorption refrigerator flows constantly and exchanges heat continuously with external heat reservoirs; (7) Work input required by the solution pump in the absorption refrigerator is negligible; (8) Heat transfers within the system obey Newton's law.

2.1. The MCFC

When the electrochemical reactions are proceeded inside the MCFC, some irreversible losses primarily originated from the anode overpotential, cathode overpotential and ohmic overpotential are inevitable. Adopted the electrochemical model proposed in Refs. [52, 53], the electric power output and efficiency of an MCFC can be, respectively, expressed as

$$P_{MCFC} = jA(E - U_{an} - U_{cat} - U_{ohm}), \tag{1}$$

and

$$\eta_{MCFC} = \frac{n_e F}{-\Delta h}\left(E - U_{an} - U_{cat} - U_{ohm}\right), \tag{2}$$

where

$$E = E_0 + \frac{RT}{n_e F}\ln\left[\frac{p_{\mathrm{H_2,an}}\left(p_{\mathrm{O_2,cat}}\right)^{0.5} p_{\mathrm{CO_2,cat}}}{p_{\mathrm{H_2O,an}}\, p_{\mathrm{CO_2,an}}}\right], \tag{3}$$

$$E_0 = \left(242000 - 45.8T\right)/(n_e F), \tag{4}$$

$$U_{an} = 2.27\times10^{-9}\, j \exp\left(\frac{E_{act,an}}{RT}\right) p_{\mathrm{H_2,an}}^{-0.42} p_{\mathrm{CO_2,an}}^{-0.17} p_{\mathrm{H_2O,an}}^{-1.0}, \tag{5}$$

$$U_{cat} = 7.505\times10^{-10}\, j \exp\left(\frac{E_{act,cat}}{RT}\right) p_{\mathrm{O_2,cat}}^{-0.43} p_{\mathrm{CO_2,cat}}^{-0.09}, \tag{6}$$

$$U_{ohm} = 0.5\times10^{-4}\, j \exp\left[3016\left(\frac{1}{T} - \frac{1}{923}\right)\right], \tag{7}$$

2.2. The absorption refrigerator

The absorption refrigerator in the hybrid system begins to extract heat from the cooled space once some waste heat flow from the MCFC to the generator. The absorption refrigerator is operated

between three temperature levels given assumptions that the working fluids in the absorber and condenser have the same temperature (i.e., T_3) and exchange heat with the heat sinks at the same temperature (i.e., T_0) [56-59]. By considering the internal irreversible effects inside the working fluids and the external finite-rate heat transfer irreversibilities, one may obtain the maximum cooling rate R and the corresponding coefficient of performance ε of the absorption refrigerator for a given heat-transfer rate q_h and total heat-transfer area A_R [57, 58]:

$$R = q_c = \frac{q_h}{2}\left\{\left[\left(a+\frac{I_rT_0-T_c}{Cq_h}\right)^2 - 4T_c\left(\frac{1}{(1+B)^2T}-\frac{1-I_rT_0/T}{Cq_h}\right)\right]^{0.5} - \left[a+\frac{I_rT_0-T_c}{Cq_h}\right]\right\}, \tag{8}$$

and

$$\varepsilon = \frac{1}{2}\left\{\left[\left(a+\frac{I_rT_0-T_c}{Cq_h}\right)^2 - 4T_c\left(\frac{1}{(1+B)^2T}-\frac{1-I_rT_0/T}{Cq_h}\right)\right]^{0.5} - \left[a+\frac{I_rT_0-T_c}{Cq_h}\right]\right\}, \tag{9}$$

where $a = 1+\left(T_c - I_rB^2T_0\right)\Big/\left[(1+B)^2T\right]$, I_r is the internal irreversibility factor that characterizes the irreversible extent inside cyclic working fluids, $B = \left(\sqrt{b_2}-1\right)\Big/\left(1+\sqrt{I_rb_1}\right)$, K_h is the heat-transfer coefficient of the generator, K_0 is the heat-transfer coefficient of the condenser or absorber, and K_c is the heat-transfer coefficient of the evaporator, $b_1 = K_h/K_0$, $b_2 = K_h/K_c$; A_0 is the total heat-transfer area of the condenser and absorber, A_h and A_c are respectively the heat-transfer areas of the generator and evaporator, $A_R = A_h + A_c + A_o$ is the overall heat-transfer area of the absorption refrigerator, $C = (1+B)^2\Big/(A_RK)$ and $K = K_h\Big/\left[1+\sqrt{I_rb_1}\right]^2$.

As the exergy contents of electric power and cooling load are different, the equivalent power output P_{AR} and efficiency η_{AR} for absorption refrigerator can be expressed as [60, 61]:

$$P_{AR} = q_c\left|1-\frac{T_0}{T_c}\right| = \frac{q_h}{2}\left|1-\frac{T_0}{T_c}\right|\left\{\left[\left(a+\frac{I_rT_0-T_c}{Cq_h}\right)^2 - 4T_c\left(\frac{1}{(1+B)^2T}-\frac{1-I_rT_0/T}{Cq_h}\right)\right]^{0.5} - \left[a+\frac{I_rT_0-T_c}{Cq_h}\right]\right\}, \tag{10}$$

and

$$\eta_{AR}=\frac{P_{AR}}{q_h}=\frac{1}{2}\left|1-\frac{T_0}{T_c}\right|\left\{\left[\left(a+\frac{I_rT_0-T_c}{Cq_h}\right)^2-4T_c\left(\frac{1}{(1+B)^2T}-\frac{1-I_rT_0/T}{Cq_h}\right)\right]^{0.5}-\left[a+\frac{I_rT_0-T_c}{Cq_h}\right]\right\}. \quad (11)$$

2.3. The regenerator

The regenerator in the hybrid system functions as a counter-flow heat exchanger that absorbers the high-temperature heat contained in the exhaust products at temperature T to warm the inlet reactants at the ambient temperature T_0. Due to the irreversibility associated with heat transfer, some regenerative losses are inevitable and the rate of regenerative losses is often calculated as follows [30, 62]:

$$q_{re}=K_{re}A_{re}(1-\varepsilon)(T-T_0), \quad (12)$$

2.4. Performance of the hybrid system

The heat-leak rate q_L is often assumed to be proportional to the temperature difference between the MCFC and the environment, thus q_L and q_1 can be, respectively, expressed as [63, 64]

$$q_L=K_LA_L(T-T_0), \quad (13)$$

and

$$q_h=-\Delta\dot{H}-P_{MCFC}-q_{re}-q_L=-\frac{A\Delta h}{2F}\left[(1-\eta_{MCFC})\,j-\frac{2F(c_1+c_2)(T-T_0)}{-\Delta h}\right], \quad (14)$$

where K_L is the heat-leakage coefficient, A_L is the corresponding heat-transfer area, $c_1=[K_{re}A_{re}(1-\varepsilon)]/A$ and $c_2=K_LA_L/A$ are two integrated parameters that not only depend on the heat-transfer irreversibilities but also depend on the geometric sizes of the regenerator and MCFC.

As shown by Eq. (14), the bottoming absorption refrigerator begins to absorb heat from the cooled space only when the formula (15) is valid

$$-\Delta \dot{H} - P_{MCFC} > q_{re} + q_L \,. \tag{15}$$

Combining Eq. (14), Eq. (15) can be explicitly rewritten as

$$j > j_C = \left[\frac{2F}{-\Delta h\left(1-\eta_{MCFC}\right)}\right]\left[\left(c_1 + c_2\right)\left(T - T_0\right)\right], \tag{16}$$

where j_C is the lower bound operating current density of the MCFC from which the bottoming absorption refrigerator starts to work. Moreover, the allowable maximum current density j_M can be numerically determined by Eqs. (12) - (14) and the condition of $P_{AR} > 0$.

For $j_C < j < j_M$, the equivalent power output P and efficiency η of the hybrid system can be, respectively, expressed as

$$P = P_{MCFC} + q_c\left|1-\frac{T_0}{T_c}\right| = P_{MCFC} + \frac{q_h}{2}\left|1-\frac{T_0}{T_c}\right|\left\{\left[\left(a+\frac{I_r T_0 - T_c}{Cq_h}\right)^2 - 4T_c\left(\frac{1}{\left(1+B\right)^2 T} - \frac{1-I_r T_0/T}{Cq_h}\right)\right]^{0.5} - \left[a+\frac{I_r T_0 - T_c}{Cq_h}\right]\right\}, \tag{17}$$

and

$$\eta = \frac{P_{MCFC} + P_{AR}}{-\Delta \dot{H}}$$

$$= \eta_{MCFC} + \frac{\left|1-\frac{T_0}{T_c}\right|}{2}\left[1-\eta_{MCFC} + \frac{2F\left(c_1+c_2\right)\left(T-T_0\right)}{j\Delta h}\right]\left\{\left[\left(a+\frac{I_r T_0 - T_c}{Cq_h}\right)^2 - 4T_c\left(\frac{1}{\left(1+B\right)^2 T} - \frac{1-I_r T_0/T}{Cq_h}\right)\right]^{0.5} - \left[a+\frac{I_r T_0 - T_c}{Cq_h}\right]\right\}. \tag{18}$$

For $j \le j_C$ or $j \ge j_M$, the absorption refrigerator in the hybrid system works totally irreversibly, $P_{AR} = 0$ and $\eta_{AR} = 0$, and the power output P and efficiency η of the hybrid system equal to that of the stand-alone MCFC, i.e.,

$$P = P_{MCFC}\,, \tag{19}$$

and

$$\eta = \eta_{MCFC} . \quad (20)$$

3. Performance characteristics and optimum operating regions

Based on the mathematical model formulated in Section 2 and typical parameters summarized in Table 1 [52, 53, 55], numerical calculations can be used to reveal the general performance characteristics of the hybrid system. The power densities and efficiencies of the MCFC, absorption refrigerator and hybrid system varying with the operating current density of MCFC are shown in Fig. 2, where $P^*_{MCFC} = P_{MCFC} / A$, $P^*_{AR} = P_{AR} / A$ and $P^* = P / A$ are, respectively, the power densities of the MCFC, absorption refrigerator and hybrid system, j_P and η_P are, respectively, the operating current density and efficiency corresponding to the hybrid system maximum power density $P^*_{\max}$, P^*_C and η_C are, respectively, the power density and efficiency at j_C, P^*_M and η_M are, respectively, the power density and efficiency at j_M, j_S is the stagnation current density from which the fuel cell does not deliver electricity any more. It is seen that P^* first increases and then decreases as j is increased, η first decreases then slightly increases and thereafter continuously decreases with j. Figure 2 also shows that j_P is always different from $j_{MCFC,\,P}$ since $j_{MCFC,\,P}$ is always different from $j_{AR,\,P}$, where $j_{MCFC,\,P}$ and $j_{AR,\,P}$ are, respectively, the current densities corresponding to the maximum power density of MCFC $P^*_{MCFC,\max}$ and the maximum power density of absorption refrigerator $P^*_{AR,\max}$. For the typical parameters given in Table 1, the hybrid system reaches $P^*_{\max}$, 1531.2 W m^{-2}, at 2943 A m^{-2}, and the MCFC reaches $P^*_{MCFC,\max}$, 1483.8 W m^{-2}, at 2959 A m^{-2}. Meanwhile, η_P and $\eta_{MCFC,\,P}$ (i.e., efficiency of MCFC at $P^*_{MCFC,\max}$) are 40.7% and 39.2%, respectively. $P^*_{\max}$ is about 3.2% larger than $P^*_{MCFC,\max}$, and η_P is about 3.8% larger than $\eta_{MCFC,\,P}$. When $0 < j \le j_C$ or $j \ge j_M$, the curves of $P^* \sim j$ and $\eta \sim j$ are overlapped with that of

$P^*_{MCFC} \sim j$ and $\eta_{MCFC} \sim j$, respectively. When the operating current density is operated in the region of $j_C < j < j_M$, both power density and efficiency of the hybrid system is greater than that of the stand-alone MCFC. This fact clearly shows that the performance of the MCFC can be effectively improved by recovering the waste heat for cooling purposes through a bottoming absorption refrigerator.

As illustrated in Fig. 2, an increasing j not only lowers P^* but also debases η in the region of $j > j_P$. Combined P^* and η together with the thermoeconomic optimization criterion [65, 66] into consideration, j is suggested to situate in the following region

$$j_C < j \le j_P . \tag{21}$$

Correspondingly, the optimum operating regions for P^* and η are, respectively, determined by

$$P^*_C < P^* \le P^*_{\max}, \tag{22}$$

and

$$\eta_C > \eta \ge \eta_P, \tag{23}$$

when the hybrid system is operated in the above regions, η increases as P^* decreases, and vice versa.

4. Results and discussion

As shown by Eqs. (17) - (20), the performance of the MCFC/absorption refrigerator hybrid system not only depends on a set of designing parameters and operating conditions such as heat-transfer coefficients (i.e., K_h, K_c and K_0), heat-transfer areas (i.e., A_h, A_c, A_0 and A_R), internal irreversibility of the absorption refrigerator I_r, polar plate area A, operating current density j, operating temperature T and operating pressure p of the MCFC, but also depends on

some thermodynamic losses related parameters (i.e., c_1 and c_2). In this section, we will discuss the effects of these parameters on the performance of the hybrid system through comprehensive parametric analyses.

4.1. Effect of internal irreversibility

The internal irreversibility $I_r = \Delta S_o / (\Delta S_h + \Delta S_c)$ is a parameter that characterizes the irreversible losses caused by mass transfer, friction, eddy and other irreversible effects inside the cyclic working fluid of the absorption refrigerator [56-58], where $\Delta S_0 = q_0 / T_3$ is the entropy rate that flows out of the cyclic working fluid, $\Delta S_h = q_h / T_1$ and $\Delta S_c = q_c / T_2$ are entropy rates that flow into the cyclic working fluids. Figure 3 shows that P and η increase as I_r decreases in the region of $j_C < j < j_M$, and j_P shifts to a larger value as I_r decreases. The detailed numerical results in Table 2 indicate that the value of j_C does not vary with I_r, while both j_M and the effective operating current density interval Δj ($= |j_M - j_C|$) increase as I_r decreases. The black solid line in Fig. 3 represents a special case that the internal irreversible effect inside the working fluid can be neglected. In such a case, Eqs. (17) and (18) can be, respectively, reduced into

$$P = P_{MCFC} + \frac{q_h}{2}\left|1-\frac{T_0}{T_c}\right|\left\{\left[\left(a_1+\frac{T_0-T_c}{C_1 q_h}\right)^2 - 4T_c\left(\frac{1}{(1+B_1)^2 T} - \frac{1-T_0/T}{C_1 q_h}\right)\right]^{0.5} - \left[a_1+\frac{T_0-T_c}{C_1 q_h}\right]\right\} \tag{24}$$

and

$$\eta = \eta_{MCFC} + \frac{\left|1-\frac{T_0}{T_c}\right|}{2}\left[1-\eta_{MCFC}+\frac{2F(c_1+c_2)(T-T_0)}{j\Delta h}\right]\left\{\left[\left(a_1+\frac{T_0-T_c}{C_1 q_h}\right)^2 - 4T_c\left(\frac{1}{(1+B_1)^2 T} - \frac{1-T_0/T}{C_1 q_h}\right)\right]^{0.5} - \left[a_1+\frac{T_0-T_c}{C_1 q_h}\right]\right\}, \tag{25}$$

where $a_1 = 1+\left(T_c - B_1^2 T_0\right)\Big/\left[(1+B_1)^2 T\right]$, $B_1 = \left(\sqrt{b_2}-1\right)\Big/\left(1+\sqrt{b_1}\right)$, $C_1 = (1+B_1)^2 \Big/ (A_R K_1)$, $K_1 = K_h \Big/ \left[1+\sqrt{b_1}\right]^2$.

4.2. Effect of heat-transfer coefficient

Heat-transfer coefficients of working fluid K_i (i = h, c and 0) dramatically affect the performance of the absorption refrigerator and thus influence the overall performance of the hybrid system. The effects of heat-transfer coefficients on the hybrid system performance are shown in Fig. 4. When j is operated in the region of $j_C < j < j_M$, P^* and η are monotonically increasing functions of K_h and monotonically decreasing functions of b_1 and b_2, j_P shifts to a larger value as K_h increases or as b_1 and/or b_2 decrease. It is seen from Fig. 4 (a) that j_C does not vary with K_h, whereas j_M and Δj increase as K_h is increased. Table 2 shows that j_C does not vary with b_1 and b_2, j_M and Δj obviously decrease as b_1 increases, but j_M and Δj slightly decreases as b_2 increases. The wine dash-dot line in Fig. 4 (a) represents a special case in which heat transfer coefficients of the absorption refrigerator tend to be infinitely large and the heat transfer irreversibilities between the working fluid and the external heat sources disappear. The black solid line in Fig. 4 (b) represents another special case that the heat-transfer coefficients K_c and K_0 trend to be infinite large (i.e., $b_1 \to 0$ and $b_2 \to 0$) for a given K_h. When heat-transfer coefficients are large enough, P^* and η can be still larger than zero even when j exceeds j_S. In this situation, the MCFC works as a heat reservoir of the absorption refrigerator rather than an electrochemical converter. The region $j > j_S$ exceeds the optimum region of $j_C < j \le j_P$ although the system may work in it. When j is operated in the region $j > j_S$, the MCFC is totally irreversible [67], and the numerical expressions for P and η are, respectively, given by

$$P = \frac{q_{h1}}{2}\left|1-\frac{T_0}{T_c}\right|\left\{\left[\left(a+\frac{I_rT_0-T_c}{Cq_{h1}}\right)^2-4T_c\left(\frac{1}{(1+B)^2T}-\frac{1-I_rT_0/T}{Cq_{h1}}\right)\right]^{0.5}-\left[a+\frac{I_rT_0-T_c}{Cq_{h1}}\right]\right\}, \tag{26}$$

and

$$\eta = \frac{\left|1-T_0/T_c\right|}{2}\left[1+\frac{2F\left(c_1+c_2\right)\left(T-T_0\right)}{j\Delta h}\right]\left\{\left[\left(a+\frac{I_rT_0-T_c}{Cq_{h1}}\right)^2-4T_c\left(\frac{1}{\left(1+B\right)^2T}-\frac{1-I_rT_0/T}{Cq_{h1}}\right)\right]^{0.5}-\left[a+\frac{I_rT_0-T_c}{Cq_{h1}}\right]\right\}, \quad (27)$$

where $q_{h1} = -\frac{A\Delta h}{n_eF}\left[j-\frac{n_eF\left(c_1+c_2\right)\left(T-T_0\right)}{-\Delta h}\right]$.

4.3. Effect of operating temperature

The operating temperature T is an important operating condition that not only affects the thermodynamic losses but also affects the performances of the MCFC and the absorption refrigerator. Different from the effects of I_r, K_h, b_1 and b_2, the effect of T on the performance of the hybrid system are in the entire range of j, as shown in Fig. 5. Both P^* and η increase as T increases, and the effect of T on the hybrid system performance becomes more significant with increasing T. Moreover, the values of j_P, j_C, j_M and Δj increase as T increases. A larger T not only increases the equilibrium potential but also reduces the anode, cathode and ohmic overpotentials, which improves the MCFC performance. In addition, a higher T creates a larger temperature difference $\left(T-T_0\right)$, which improves the absorption refrigerator performance and also causes larger thermodynamic losses simultaneously. As the performance enhancements in MCFC and absorption refrigerator are greater than the performance reduction resulting from the thermodynamic losses, a larger T is always preferable.

4.4. Effect of thermodynamic losses related parameters

The thermodynamic losses are not only related to the temperature gap between T and T_0 but also associated with the integrated parameters c_1 and c_2. As shown in Fig. 6 (a), the curves of $P_{AR}^* \sim j$ and $\eta_{AR} \sim j$ move rightward and $P_{AR,\max}^*$ almost keeps invariant as c_1 and/or c_2 are increased. Both j_C and j_M increase as c_1 and/or c_2 are increased, while Δj decreases as c_1

and/or c_2 increase. As P_{MCFC}^* and η_{MCFC} are neither influenced by c_1 nor affected by c_2, P^* and η decrease at low current densities and increase at large current densities as c_1 and/or c_2 are increased, as shown in Fig. 6 (b). When c_1 and/or c_2 are larger enough, e.g., the wine dash-dot line case represented in Fig. 6, j_M may exceeds j_S. For this situation, the numerical expressions for P and η can be, respectively, expressed by Eqs. (26) and (27). The black solid lines in Fig. 6 represent a special case that the thermodynamic losses q_r and q_L can be negligible (i.e., $c_1 = 0$ and $c_2 = 0$). In this case, the bottoming absorption refrigerator starts to absorb heat from the cooled space once the MCFC is put into operation, and Eqs. (14) and (16) can be, respectively, reduced into

$$q_h = -\frac{jA\left(1-\eta_{MCFC}\right)\Delta h}{2F}, \tag{28}$$

and

$$j > j_C = 0. \tag{29}$$

4.5. Effect of operating pressure

Similar to the effects of operating temperature T, the operating pressure p not only affects the MCFC performance but also affects the amount of waste heat transferred from the MCFC to the absorption refrigerator. The effect of p on the performance of the hybrid system is in the entire range of j, as shown in Fig. 7. Both P^* and η increase as p increases, and the effect of p on the hybrid system performance becomes more significant as p increases. Additionally, the values of j_P, j_C, j_M, j_S and Δj increase with a larger p. Although a larger p benefits performance improvement, it also cost more electricity to compress the inlet reactants. The ambient operating pressure is the usual choice, as represented by the black solid line in Fig. 7.

5. Conclusions

An MCFC-based absorption refrigerator hybrid system was put forward to harvest the waste heat in the MCFC for cooling purposes. The effective operating current density interval of the MCFC permits the absorption refrigerator to function was determined and numerical expressions to evaluate the performance of the hybrid system were specified. It was found that the performance of the MCFC could be effectively improved by integrating with an absorption refrigerator. The general performance characteristics and optimum operating regions for the hybrid system were revealed. The effects of the operating current density, operating temperature and operating pressure of the MCFC, internal irreversibility and heat transfer coefficients of the absorption refrigerator, and some thermodynamic losses related parameters on the performance of the hybrid system were discussed by comprehensive parametric studies. The results obtained in the paper may offer some theoretical guidance for performance improvement of MCFCs through cogeneration systems.

Acknowledgements

This work has been supported by the Natural Science Foundation of Zhejiang Province of China (Grant No. LQ14E06002), the National Natural Science Foundation of China (Grant No. 51406091), the Zhejiang Open Foundation of the Most Important Subjects (Grant No. xkzw108), and The Hong Kong Polytechnic University Research Project (Grant No. 1-YW1F).

References

[1] Kirubakaran A, Jain S, Nema RK. A review on fuel cell technologies and power electronic interface. Renew Sust Energy Rev 2009;13:2430-40.

[2] Acres GJK. Recent advances in fuel cell technology and its applications. J Power Sources 2001;100:60-6.

[3] Sharaf OZ, Orhan MF. An overview of fuel cell technology: Fundamentals and applications. Renew Sust Energy Rev 2014;32:810-53.

[4] Bischoff M. Molten carbonate fuel cells: A high temperature fuel cell on the edge to commercialization. J Power Sources 2006;160:842-5.

[5] Antolini E. The stability of $LiAlO_2$ powders and electrolyte matrices in molten carbonate fuel cell environment. Ceram Int 2013;39:3463-78.

[6] Wu S, Zhang H, Ni M. Performance assessment of a hybrid system integrating a molten carbonate fuel cell and a thermoelectric generator. Energy 2016;112:520-7.

[7] Kim H, Bae J, Choi D. An analysis for a molten carbonate fuel cell of complex geometry using three-dimensional transport equations with electrochemical reactions. Int J Hydrogen Energy 2013;38:4782-91.

[8] Ramandi MY, Dincer I, Berg P. A transient analysis of three-dimensional heat and mass transfer in a molten carbonate fuel cell at start-up. Int J Hydrogen Energy 2014;39:8034-47.

[9] Heidebrecht P, Sundmacher K. Dynamic modeling and simulation of a countercurrent molten carbonate fuel cell (MCFC) with internal reforming. Fuel Cells 2003;2:166-80.

[10] Pfafferodt M, Heidebrecht P, Sundrmacher K. Stack modeling of a molten carbonate fuel cell (MCFC). Fuel Cells 2010;10:619-35.

[11] Law MC, Lee VCC, Tay CL. Dynamic behaviors of a molten carbonate fuel cell under a sudden shut-down scenario: The effects on temperature gradients. Appl Therm Eng 2015;82:98-109.

[12] Wee JH. Carbon dioxide emission reduction using molten carbonate fuel cell system. Renew Sust Energy Rev 2014; 32:178-91.

[13] Campanari S, Chiesa P, Manzolini G. CO_2 capture from combined cycles integrated with Molten Carbonate Fuel Cells. Int J Greenh Gas Control 2010; 4:441-51.

[14] Hu L, Rexed I, Lindbergh G, Lagergren C. Electrochemical performance of reversible molten carbonate fuel cells. Int J Hydrogen Energy 2014;39:12323-9.

[15] Donado RA, Marianowski LG, Maru HC, Selman JR. Corrosion of the wet-seal area in molten carbonate fuel cells I. Analysis. J Electrochem Soc 1984;131:2535-40.

[16] Mehmeti A, Santoni F, Pietra MD, McPhail SJ. Life cycle assessment of molten carbonate fuel cells: State of the art and strategies for the future. J Power Sources 2016;308:97-108.

[17] Campanari S, Chiesa P, Manzolini G, Bedogni S. Economic analysis of CO_2 capture from natural gas combined cycles using Molten Carbonate Fuel Cells. Appl Energy 2014;130:562-73.

[18] Zervas P L, Koukou M K, Markatos N C. Predicting the effects of process parameters on the performance of phosphoric acid fuel cells using a 3-D numerical approach. Energy Convers Managem 2006;47:2883-99.

[19] Yoshiba F, Ono N, Izaki Y, Watanabe T, Abe T. Numerical analyses of the internal conditions of a molten carbonate fuel cell stack: comparison of stack performances for various gas flow types. J Power Sources 1998;71:328-36.

[20] Bae SJ, Ahn Y, Lee J, Lee JI. Various supercritical carbon dioxide cycle layouts study for molten carbonate fuel cell application. J Power Sources 2014;270:608-18.

[21] Giulio ND, Bosio B, Han J, McPhail SJ. Experimental analysis of SO_2 effects on molten carbonate fuel cells. Int J Hydrogen Energy 2014;39:12300-8.

[22] Melendez-Ceballos A, Albin V, Femandez-Valverde SM, Ringuede A, Cassir M. Electrochemical properties of Atomic layer deposition processed CeO_2 as a protective layer for the molten carbonate fuel cell cathode. Electrochim Acta 2014;174-81.

[23] Kulkarni A, Giddey S. Materials issues and recent developments in molten carbonate fuel cells. J Solid State Electrochem 2012;16:3123-46.

[24] Zhang X, Guo J, Chen J. Influence of multiple irreversible losses on the performance of a molten carbonate fuel cell-gas turbine hybrid system. Int J Hydrogen Energy 2012;37:8664-71.

[25] De Lorenzo G, Fragiacomo P. A Methodology for improving the performance of molten carbonate fuel cell/gas hybrid systems. Int J Energy Res 2012;36:96-110.

[26] EI-Emam RS, Dincer I. Energy and exergy analyses of a combined molten carbonate fuel cell – Gas turbine system. Int J Hydrogen Energy 2011;36:8927-35.

[27] Wee JH. Molten carbonate fuel cell and gas turbine hybrid systems as distributed energy resources. Appl Energy 2011;88:4252-63.

[28] Greppi P, Bosio B, Arato E. Feasibility of the integration of a molten carbonate fuel cell system and an integrated gasification combined cycle. Int J Hydrogen Energy 2009;34:8664-9.

[29] Grillo O, Magistri L, Massardo AF. Hybrid systems for distributed power generation based on pressurization and heat recovering of an existing 100 kW molten carbonate fuel cell. J Power Sources 2003;115:252-67.

[30] Zhang H, Lin G, Chen J. Performance evaluation and parametric optimum criteria of an irreversible molten carbonate fuel cell-heat engine hybrid system. Int J Electrochem Sci

2011;4714-29.

[31] Zhang H, Su S, Lin G, Chen J. Performance analysis and multi-objective optimization of a molten carbonate fuel cell-Braysson heat engine hybrid system. Int J Electrochem Sci 2012;7:3420-35.

[32] Sánchez D, Chacartegui R, Torres M, Sánchez T. Stirling based fuel cell hybrid systems: An alternative for molten carbonate fuel cells. J Power Sources 2009;192:84-93.

[33] Vatani A, Khazaeli A, Roshandel R, Panjeshahi MH. Thermodynamic analysis of application of organic Rankine cycle for heat recovery from an integrated DIR-MCFC with preformer. Energy Convers Managem 2013;67:197-207.

[34] Mamaghani AH, Najafi B, Shirazi A, Rinaldi F. 4E analysis and multi-objective optimization of an integrated MCFC (molten carbonate fuel cell) and ORC system. Energy 2015;82:650-63.

[35] Zhang X, Wang Y, Guo J, Shih TM, Chen J. A unified model of high-temperature fuel-cell heat-engine hybrid systems and analyses of its optimum performances. Int J Hydrogen Energy 2014;39:1811-25.

[36] Parise JAR, Pitanga Marques R. The role of heat transfer in refrigeration. Heat Transfer Eng 2005;26:1-4.

[37] Pan QW, Wang RZ, Wang LW. Comparison of different kinds of heat recoveries applied in adsorption refrigeration system. Int J Refrigeration 2015;55:37-48.

[38] Ahmadi MH, Ahmadi MA, Mehrpooya M, Hosseinzade H, Feidt M. Thermodynamic and thermo-economic analysis and optimization of performance of irreversible four-temperature-level absorption refrigeration. Energy Convers Managem 2014;88: 1051-9.

[39] Ahmadi MH, Ahmadi MA, Sadatsakkak SA. Thermodynamic analysis and performance

optimization of irreversible Carnot refrigerator by using multi-objective evolutionary algorithms (MOEAs). Renew Sust Energy Rev 2015; 51 : 1055-70.

[40] Ahmadi MH, Ahmadi MA, Feidt M. Thermodynamic analysis and evolutionary algorithm based on multi-objective optimization of performance for irreversible four-temperature-level refrigeration. Mech Ind 2015; 16: 207.

[41] Nouadje BAM, Ngouateu Wouagfack PA, Tchinda R. Finite-time thermodynamics optimization of an irreversible parallel flow double-effect absorption refrigerator. Int J Refrigeration 2016;67: 433-44.

[42] Ahmadi MH, Ahmadi MA, Mohammadi AH, Feidt M, Pourkiaei SM. Multi-objective optimization of an irreversible Stirling cryogenic refrigerator cycle. Energy Convers Managem 2014; 82:351-60.

[43] Bellos E, Tzivanidis C, Antonopoulos KA. Exergetic, energetic and financial evaluation of a solar driven absorption cooling system with various collector types. Appl Therm Eng 2016;102:749-59.

[44] Kalinowski P, Hwang Y, Radermacher R, Hashimi SA, Redgers P. Application of waste heat powered absorption refrigeration system to the LNG recovery process. Int J Refrigeration 2009;32:687-94.

[45] Talbi M, Agnew B. Energy recovery from diesel engine exhaust gases for performance enhancement and air conditioning. Appl Therm Eng 2002;22:693-702.

[46] Lu Y, Wang Y, Dong C, Wang L, Roskilly AP. Design and assessment on a novel integrated system for power and refrigeration using waste heat from diesel engine. Appl Therm Eng 2015;591-9.

[47] Yang P, Zhang H, Hu Z. Parametric study of a hybrid system integrating a phosphoric acid fuel cell with an absorption refrigerator for cooling purposes. Int J Hydrogen Energy 2016; 41: 3579-90.

[48] Wouagfack, PAN, Tchinda R. Optimal performance of an absorption refrigerator based on maximum ECOP. Int J Refrigeration 2014; 40: 404-15.

[49] Wouagfack, PAN, Tchinda R. Finite-time thermodynamics optimization of absorption refrigeration systems: A review. Renew Sust Energy Rev 2013; 21: 524-36.

[50] Wouagfack, PAN, Tchinda R. Irreversible three-heat-source refrigerator with heat transfer law of $Q \propto \Delta\left(T^{-1}\right)$ and its performance optimization based on ECOP criterion. Energy Syst 2011;2: 359-76.

[51] Silveira JL, Leal EM, Ragonha Jr LF. Analysis of a molten carbonate fuel cell: cogeneration to produce electricity and cold water. Energy 2001;26:891-904.

[52] Brouwer J, Jabban F, Leal EM, Orr T. Analysis of a molten carbonate fuel cell: Numerical modeling and experimental validation. J Power Sources 2006;158:213-24.

[53] Zhang H, Lin G, Chen J. Performance analysis and multi-objective optimization of a new molten carbonate fuel cell system. Int J Hydrogen Energy 2011;36:4015-21.

[54] Nouadje BAM, Wouagfack PAN, Tchinda R. Influence of two internal irreversibilities on the new thermo-ecological criterion for three-heat-source absorption refrigerators. Int J Refrigeration 2014;38:118-27.

[55] Ahmadi MH, Ahmadi MA. Multi objective optimization of performance of three-heat-source irreversible refrigerators based algorithm NSGAII. Renew Sust Energy Rev 2016;60:784-94.

[56] Wouagfack PAN, Tchinda R. Performance optimization of three-heat-source irreversible refrigerators based on a new thermo-ecological criterion. Int J Refrigeration 2011;34:1008-15.

[57] Lin G, Yan Z. The optimal performance of an irreversible absorption refrigerator. J Phys D: Appl Phys 1997; 2006-11.

[58] Lin G, Yan Z. The optimal operating temperature of the collector of an irreversible solar-driven refrigerator. J Phys D: Appl Phys 1999;32:94-8.

[59] Qin X, Chen L, Ge Y, Sun F. Finite time thermodynamic studies on absorption thermodynamic cycles: A state-of-the-art review. Arab J Sci Eng 2013;38:405-19.

[60] Zhang X, Chen J. Maximum equivalent power output and performance optimization of an alkaline fuel cell/heat-driven cycle hybrid system. J Power Sources 2011;196:10088-93.

[61] Chen X, Wang Y, Zhao Y, Zhou Y. A study of double functions and load matching of a phosphoric acid fuel cell/heat-driven refrigerator hybrid system. Energy 2016;101:359-65.

[62] Zhao M, Zhang H, Hu Z, Zhang Z, Zhang J. Performance characteristics of a direct carbon fuel cell/thermoelectric generator hybrid system. Energy Convers Managem 2015;89:683-9.

[63] Zhang X, Chen X, Lin B, Chen J. Maximum equivalent efficiency and power output of a PEM fuel cell/refrigeration cycle hybrid system. Int J Hydrogen Energy 2011;36:2190-6.

[64] Chen X, Wang Y, Zhou Y. Equivalent power output and parametric optimum design of a PEM fuel cell-based hybrid system. Int J Elec Power Energy Sys 2014;63:429-33.

[65] Marechal F, Palazzi F, Godat J, Favrat D. Thermo-economic modeling and optimization of fuel cell systems. Fuel Cells 2005;5:5-24.

[66] Cheddie DF. Thermo-economic optimization of an indirectly coupled solid oxide fuel cell/gas turbine hybrid power plant. Int J Hydrogen Energy 2011;36:1702-9.

[67] Zhao Y, Chen J. Modeling and optimization of a typical fuel cell-heat engine hybrid system and its parametric design criteria. J Power Sources 2009;186:96-103.

Table captions

Table 1. Parameters used in the model [52, 53, 55].

Table 2. The values of j_C, j_M, Δj, $P^*_{\max}$, j_P for different values of I_r, b_1 and b_2, where the unmentioned parameters are given in Table 1.

Figure captions

Fig. 1. Schematic diagram of an MCFC/absorption refrigerator hybrid system.

Fig. 2. Curves of (a) power densities and (b) efficiencies of the MCFC, absorption refrigerator, and hybrid system varying with the operating current density of the MCFC, where $P^*_{MCFC} = P_{MCFC} / A$, $P^*_{AR} = P_{AR} / A$ and $P^* = P / A$ are, respectively, the power densities of the MCFC, absorption refrigerator and hybrid system; η_{MCFC}, η_{AR} and η are, respectively, the efficiencies of the MCFC, absorption refrigerator and hybrid system; j_P is the operating current density at the maximum power density of hybrid system $P^*_{\max}$, j_C and j_M are, respectively, the lower bound density and upper bound current density between which the absorption refrigerator functions, P^*_C and η_C are, respectively, the power density and efficiency at j_C, P^*_M and η_M are, respectively, the power density and efficiency at j_M.

Fig. 3. Effect of internal irreversibility I_r on the performance of the hybrid system.

Fig. 4. Effect of (a) heat transfer coefficient K_h, and (b) b_1 and b_2 on the performance of the hybrid system.

Fig. 5. Effect of operating temperature T on the performance of the hybrid system.

Fig. 6. Effect of thermodynamic losses related parameters c_1 and c_2 on the performance of (a) absorption refrigerator, and (b) the hybrid system.

Fig. 7. Effect of operating pressure p on the performance of the hybrid system.

Table 1.

Parameter	Value
Faraday constant, F (C mol^{-1})	96,485
Number of electrons, n_e	2
Universal gas constant, R (J mol^{-1} K^{-1})	8.314
Operating temperature, T (K)	893
Operating pressure, p (atm)	1.0
Anode gas compositions	60%H_2/15%CO_2/25%H_2O
Cathode gas compositions	59%N_2/8%O_2/8CO_2/25%H_2O
Activation energy in the anode, $E_{act,an}$ (J mol^{-1})	53500
Activation energy in the cathode, $E_{act,cat}$ (J mol^{-1})	77300
Effective polar plate area of the MCFC, A (m^2)	0.005
Operating temperature, T (K)	893
Temperature of cooled space, T_c (K)	293
Temperature of environment, T_0 (K)	313
Internal irreversibility of absorption refrigerator, I_r	1.1
Overall heat-transfer area of absorption refrigerator, A_R (m^2)	0.0001
Heat-transfer coefficient of the generator, K_h (W K^{-1} m^{-2})	1163
Constant, c_1 (W K^{-1} m^{-2})	0.1
Constant, c_2 (W K^{-1} m^{-2})	0.1
Constant b_1	1.0
Constant b_2	1.0

Table 2.

I_r	b_1	b_2	j_C	j_M	Δj	$P^*_{\max}$	j_P
1.0	1.0	0.1	346	5599	5253	1576.9	2942
		1.0	346	5599	5253	1540.2	2942
		∞	346	5580	5234	1483.8	2959
	10	0.1	346	3709	3363	1504.8	2898
		1.0	346	3709	3363	1500.1	2910
		∞	346	3641	3295	1483.8	2959
	∞	0.1	-	-	-	1483.8	2959
		1.0	-	-	-	1483.8	2959
		∞	-	-	-	1483.8	2959
1.1	1.0	0.1	346	5357	5011	1558.3	2945
		1.0	346	5357	5011	1531.2	2943
		∞	346	5307	4961	1483.8	2959
	10	0.1	346	3520	3174	1498.6	2899
		1.0	346	3520	3174	1495.5	2910
		∞	346	3518	3172	1483.8	2959
	∞	0.1	-	-	-	1483.8	2959
		1.0	-	-	-	1483.8	2959
		∞	-	-	-	1483.8	2959
1.5	1.0	0.1	346	4426	4080	1513.4	2939
		1.0	346	4426	4080	1505.5	2940
		∞	346	4421	4075	1483.8	2959
	10	0.1	346	2828	2482	1483.8	2959
		1.0	346	2828	2482	1483.8	2959
		∞	346	2804	2458	1483.8	2959
	∞	0.1	-	-	-	1483.8	2959
		1.0	-	-	-	1483.8	2959
		∞	-	-	-	1483.8	2959

Fig. 1.

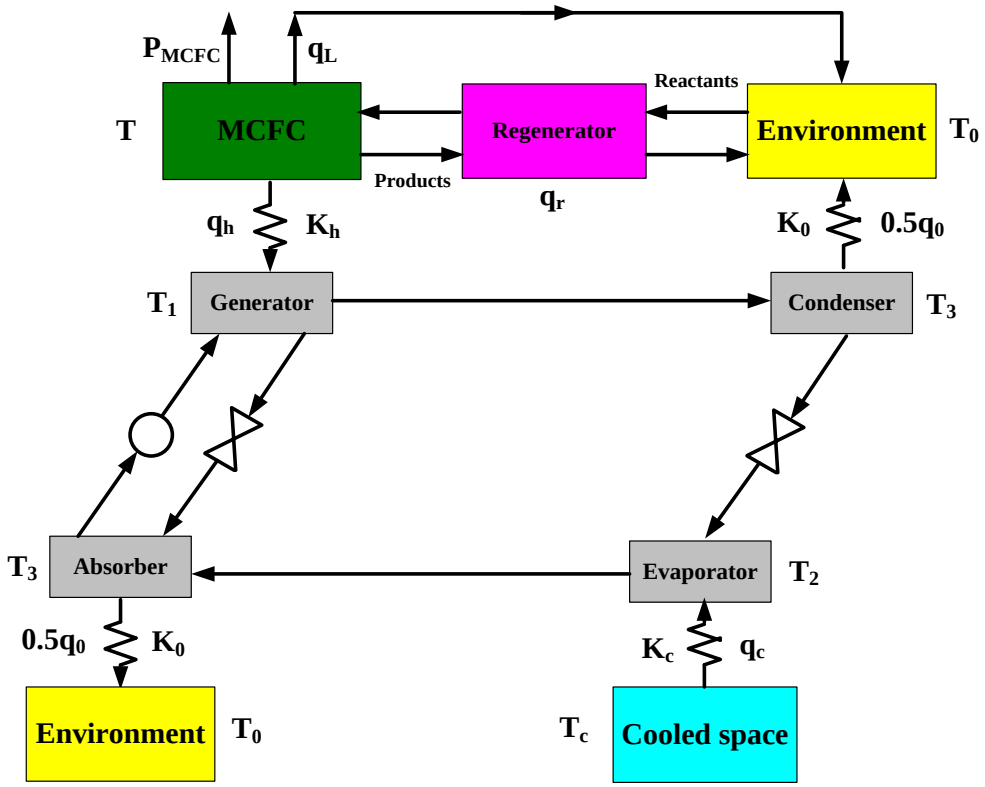

Schematic diagram of an MCFC/absorption refrigerator hybrid system.

Fig. 2.

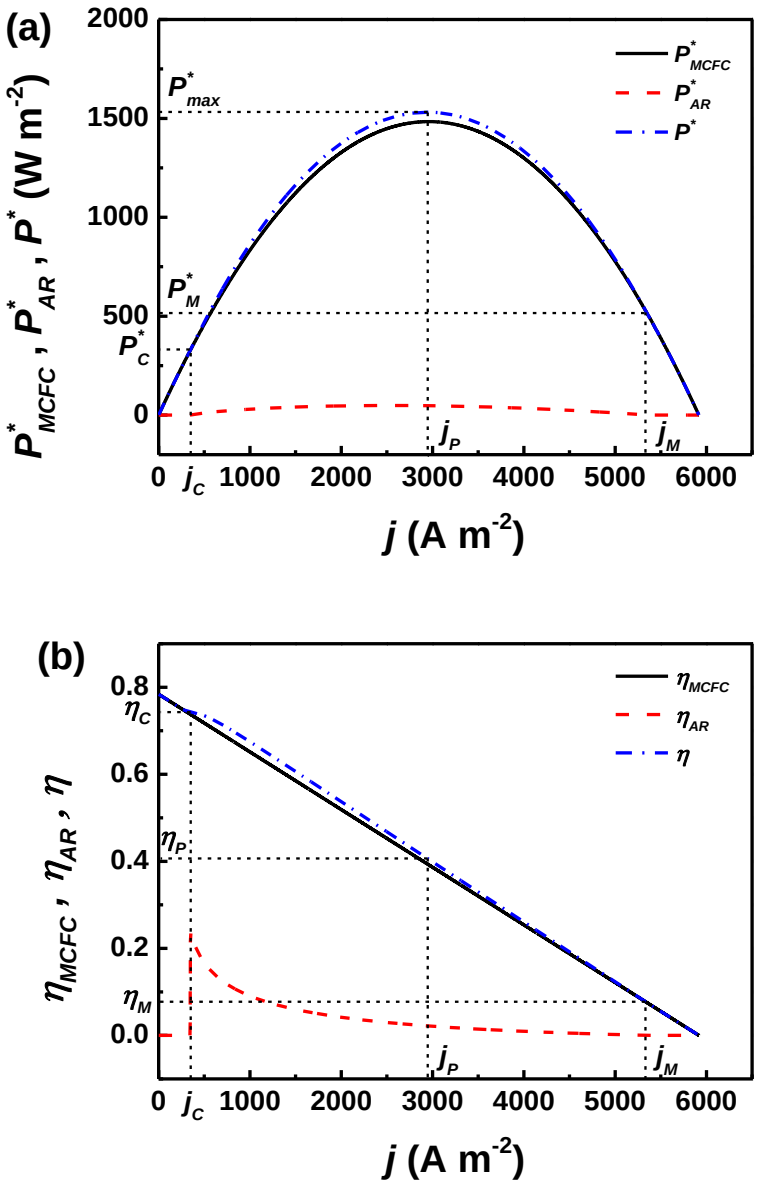

Curves of (a) power densities and (b) efficiencies of the MCFC, absorption refrigerator, and hybrid system varying with the operating current density of the MCFC, where $P^*_{MCFC} = P_{MCFC} / A$, $P^*_{AR} = P_{AR} / A$ and $P^* = P / A$ are, respectively, the power densities of the MCFC, absorption refrigerator and hybrid system; η_{MCFC}, η_{AR} and η are, respectively, the efficiencies of the MCFC, absorption refrigerator and hybrid system; j_P is the operating current density at the maximum power density of hybrid system $P^*_{\max}$, j_C and j_M are,

respectively, the lower bound density and upper bound current density between which the absorption refrigerator functions, P_C^* and η_C are, respectively, the power density and efficiency at j_C, P_M^* and η_M are, respectively, the power density and efficiency at j_M.

Fig. 3.

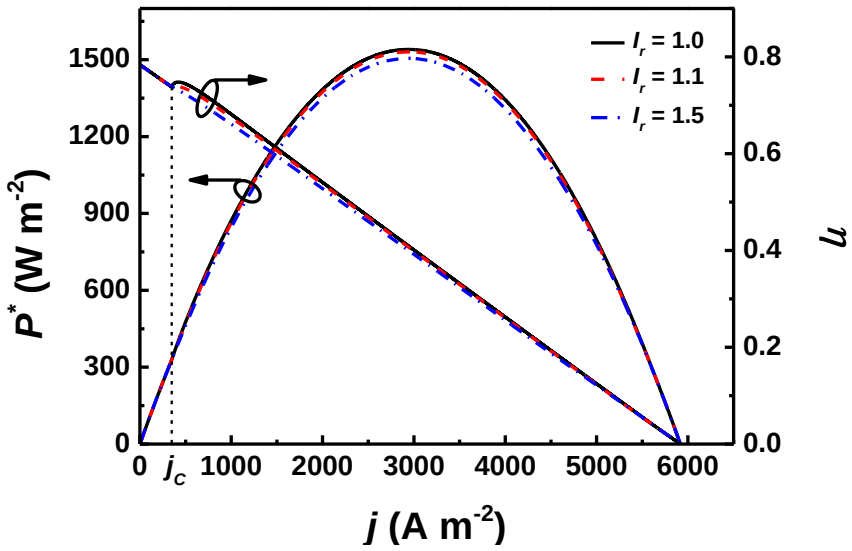

Effect of internal irreversibility I_r on the performance of the hybrid system.

Fig. 4.

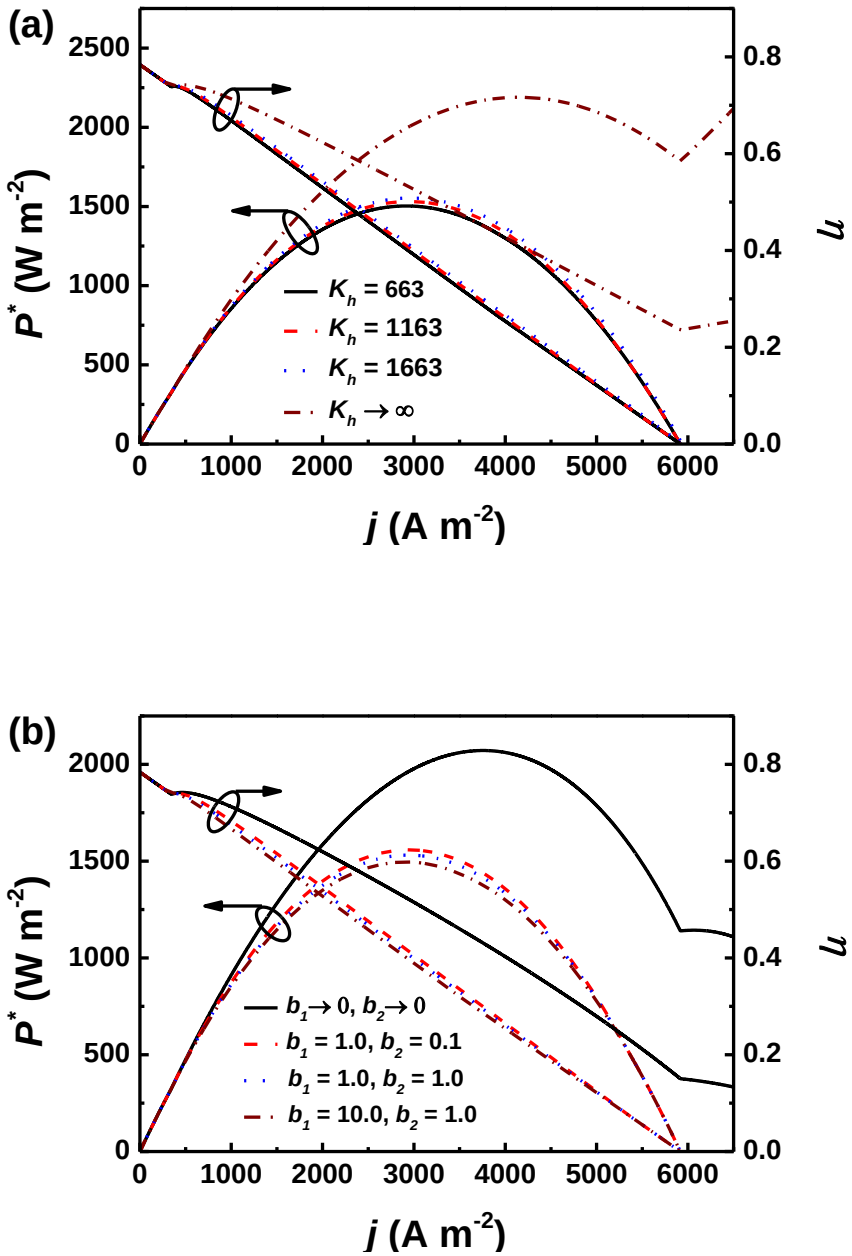

Effect of (a) heat transfer coefficient K_h, and (b) b_1 and b_2 on the performance of the hybrid system.

Fig. 5.

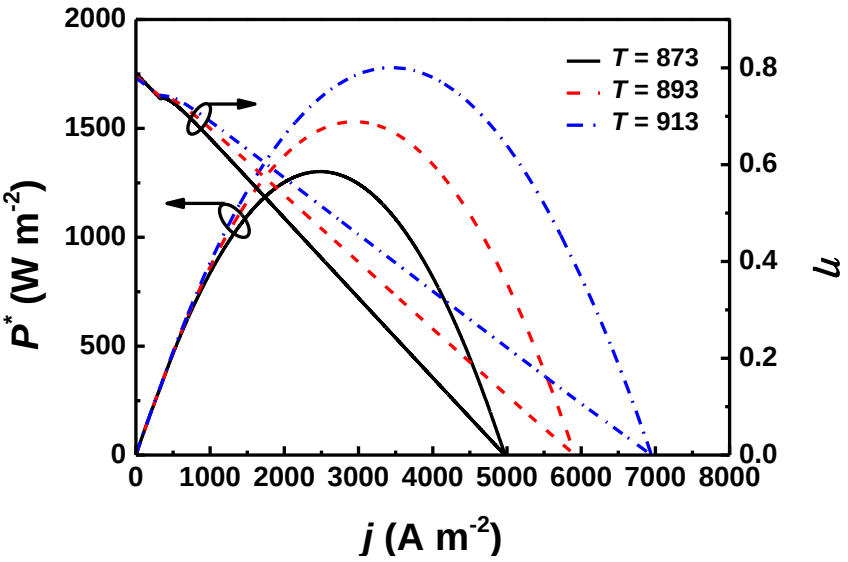

Effect of operating temperature T on the performance of the hybrid system.

Fig. 6.

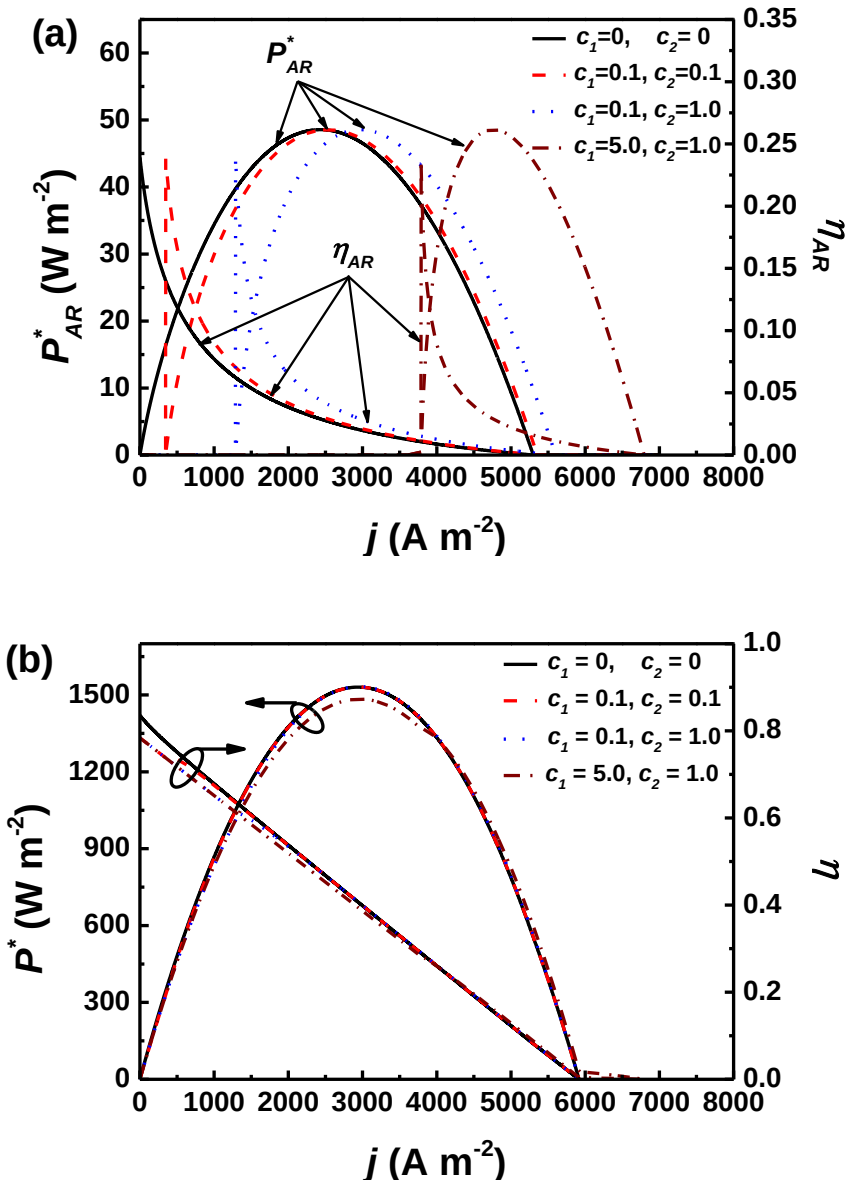

Effect of thermodynamic losses related parameters c_1 and c_2 on the performance of (a) absorption refrigerator, and (b) the hybrid system.

Fig. 7.

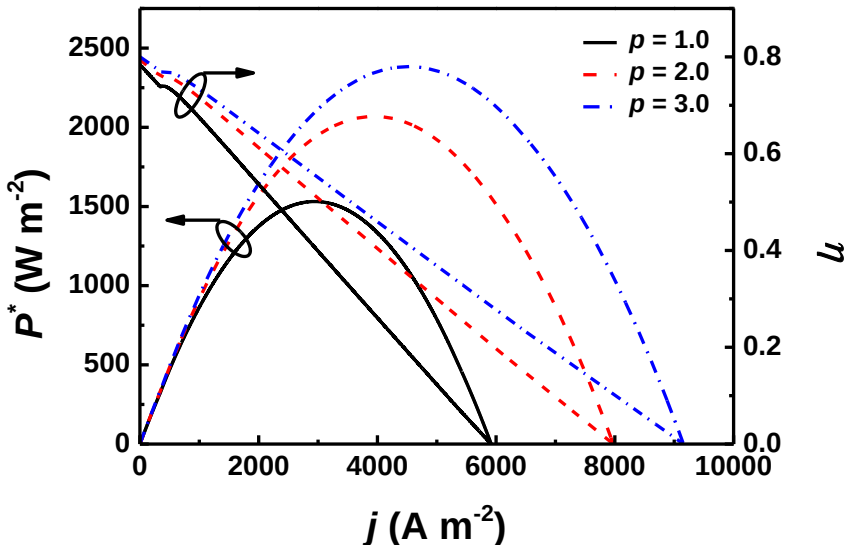

Effect of operating pressure p on the performance of the hybrid system.